IEEE Access
Multidisciplinary ⋮ Rapid Review ⋮ Open Access Journal

Received 21 November 2023, accepted 12 December 2023, date of publication 18 December 2023,
date of current version 27 December 2023.

Digital Object Identifier 10.1109/ACCESS.2023.3344398

RESEARCH ARTICLE

Wireless Power Transfer Systems With Composite Cores for Magnetic Field Shielding With Electric Vehicles

XIANYI DUAN[1], (Student Member, IEEE), JUNQING LAN[2], (Member, IEEE), SACHIKO KODERA[1], (Member, IEEE), JENS KIRCHNER[3], (Senior Member, IEEE), GEORG FISCHER[3], (Senior Member, IEEE), AND AKIMASA HIRATA[1,4], (Fellow, IEEE)

[1]Department of Electrical and Mechanical Engineering, Nagoya Institute of Technology, Nagoya 466-8555, Japan
[2]College of Electronic Engineering, Chengdu University of Information Technology, Chengdu 610103, China
[3]Institute for Electronics Engineering, Friedrich-Alexander-Universität Erlangen-Nürnberg (FAU), 91058 Erlangen, Germany
[4]Center of Biomedical Physics and Information Technology, Nagoya Institute of Technology, Nagoya 466-8555, Japan

Corresponding author: Akimasa Hirata (ahirata@nitech.ac.jp)

This work was supported in part by the Japan Society for the Promotion of Science (JSPS), Japanese–German Graduate Externship, under Grant 2019/R1; and in part by Deutsche Forschungsgemeinschaft (DFG) under Grant GRK2495/A.

ABSTRACT The transmitting and receiving coils used in wireless power transfer (WPT) systems in electric vehicles (EVs) have a larger air gap (∼300 mm) and higher transmission power (kW) than those in typical WPT systems used in electrical appliances. However, this could weaken the magnetic field, reduce transfer efficiency, and lead to a public concern regarding potential adverse health effects related to electromagnetic field (EMF) exposure. Therefore, the assessment of compliance with product safety standards, based on international exposure guidelines such as the International Commission on Non-Ionizing Radiation Protection (ICNIRP), is crucial. This study uses the finite element method to analyze a commonly used core-less and core-based WPT system using a composite core material in EVs and scalar potential finite difference method for assessment of human protection. Based on the computational results, two core structures using different types of intermediate insert blocks were analyzed to reduce external magnetic fields and mitigate the human EMF exposure. The WPT system with a core structure improved the transfer efficiency by 34% for a 300 mm air gap over the core-less system. Moreover, this effectively reduced magnetic field leakage by 91.6% and induced electric field by 98.3%, resulting in the reduction of induced electric field in anatomical human body model. The results demonstrated that a WPT system with a composite core can simultaneously improve the transfer efficiency and protect humans from EMF exposure.

INDEX TERMS EV WPT system, electromagnetic interaction, finite-element method, inductive coupling, induced electric field, wireless power transfer.

I. INTRODUCTION

As the demand for electric vehicles (EVs) continues to increase, the effective and safe recharging of batteries without human intervention has become essential. However, traditional plug-in charging, which is widely used, can potentially result in electrical leakage under wet conditions, which in turn may pose safety and hazards on human [1]. By contrast wireless power transfer (WPT) technology can effectively mitigate health concerns by enabling charging without physical contact and wired connections. Based on the inherent advantages associated with WPT technology, including convenience, low maintenance cost, advancements in reliability, and the ability to achieve full automation, this technology has been extensively used for charging EV batteries, household devices, and biomedical implants [2], [3], [4].

An inductive power transfer (IPT) system based on magnetic coupling is more suitable for medium- to high-power

The associate editor coordinating the review of this manuscript and approving it for publication was Agustin Leobardo Herrera-May.

near-field applications than other types of WPT systems [5], [6], [7], [8]. An IPT system could efficiently transfer power between two coils: one in the charging pad transmitter and the other in the vehicle receiver [9]. However, magnetic field leakage increases as the transfer distance between the two coils increases, thus reducing efficiency.

To protect humans from the adverse effects of magnetic field leakage, several international organizations have established product standards based on exposure standards [10], [11]. For example, the International Electrotechnical Commission (IEC) has published the IEC 61980 standard [12], [13], [14]. IEC-61980-1, 2, and 3 are related to general requirements, communication, and magnetic field requirements, respectively. According to these standards, the operating frequency for wireless charging systems of light-duty vehicles is 85 kHz [15]. Meanwhile, the Society of Automotive Engineers (SAE), through SAE J2954 [16], recommends three standard power levels: WPT1 at 3.7 kW, WPT2 at 7.7 kW, and WPT3 at 11 kW. Moreover, the WPT4 design standard at 22 kW is currently under development. In addition, many studies have been conducted on compliance assessment for kW order transmission [17], [18], [19]. As in vivo measurements cannot be performed, computational human body models have been widely used for the assessment of induced electric field, for example, in these international standards (e.g., IEC 61980 and SAE J2954). Such compliance assessment for product safety standards, which are based on international exposure standard (human protection) [10], [20], is crucial. These standards also provide the data gap for future studies [21].

However, despite substantial efforts, numerous issues related to the adverse effects of WPTs on humans remain to be addressed. Specifically, the issue of EMF exposure for people in close proximity to WPT systems needs to be resolved. The main goal of this study is to evaluate the performance of WPT systems used in EVs by using composite core materials and changing the core center part design simultaneously achieve improved transfer efficiency and enhanced magnetic field shielding. This study considers three types of planar ferrite cores for designing IPT systems for EVs. First, the transmission efficiency of the proposed WPT systems is calculated using the finite element method (FEM), where the vehicle body is not considered. Second, considering the exposure scenario of a human body standing nearby the vehicle, the scalar-potential-finite-difference (SPFD) method is used to assess the induced electric field in an anatomical human body to determine the assess margin of exposure limits.

This study is organized as follows: Section II presents relevant research on IPT systems and human protection. Section III the core material and designs for the proposed WPT system, the vehicle chassis, and an anatomical human body model and presents the simulation methods and exposure scenarios of this study. Section IV evaluates the performance of four WPT systems and compares the proposed system magnetic field distribution with and without the vehicle model; furthermore, a comparison of the induced field distribution in the anatomical human body model with respect to the four WPT systems is presented in this section. Section V discusses the performance, external magnetic field, and induced electric field of the four WPT systems; and Section VI describes the main conclusions of this study.

II. RELATED STUDIES

A. COIL AND CORE STRUCTURE IN INDUCTIVE POWER TRANSFER SYSTEM FOR EVS

IPT coil configurations such as circular [22], square [23], and double D [24] have been widely used to achieve high coupling efficiency between coils, thereby maximizing power transfer efficiency and minimizing losses. Among these configurations, the circular flat spiral coil configuration has gained popularity in IPT studies because of its high-power transfer performance [25]. Previous studies [26], [27] have reported that the highest power transfer efficiency can be achieved using a pair of planar spiral coils with the same diameter. Moreover, for a pair of planar coils having same inner and outer diameters, a minimum efficiency of 80% can be achieved when the inner-to-outer diameter ratio is < 0.5 [28].

Human safety can be compromised as magnetic field leakage increases. To solve the forementioned problems, ferrite cores, including E- and U-type cores, were initially proposed to reduce leakage by reshaping the magnetic path [29]. However, owing to the high cost, large weight, and poor misalignment toleration of these cores, ferrite cores with different structures and materials were proposed. A previous study proposed a circular core structure to reduce core thickness and magnetic flux leakage [30]. Then, double-D Quadrature [31], H-shaped [32], and tripolar pad core [33] structures were introduced to solve the misalignment problem. Tapered cores have also been explored because these provide good alignment tolerance and coupling coefficients [34]. Furthermore, some studies [6], [35], [36] have described the use of the optimal core thickness and coil shape to increase system performance and resilience against misalignment. In addition, aluminum plates are also acting as crucial part along with ferrite cores [37], [38]. However, these studies focused on system design, with limited attention to the adverse effects of magnetic field leakage on humans.

B. CORE MATERIAL IN IPT SYSTEM FOR EVS

According to previous research [39], manganese–zinc and nickel–zinc ferrites are the most commonly used soft magnetic materials in IPT systems because of their ability to improve performance, particularly at high frequencies ($\sim$3 GHz). These materials exhibit a combination of high magnetic permeability and low electrical conductivity, which effectively reduces the occurrence of eddy currents. Moreover, additional studies [40], [41], [42] have investigated alternative materials and their impact on the performance of

WPT systems. For instance, a previous study [40] explored the use of amorphous magnetic materials in IPT coils, demonstrating their potential for improved power transfer efficiency. A previous study [41] investigated the application of nanocrystalline magnetic materials, which reduced eddy losses compared to traditional ferrites. Another study [42] explored the use of novel magnetic composite materials in WPT systems, demonstrating their potential to increase coupling and reduce losses. However, although a high-permeability magnetic core can reduce magnetic reluctance and orient the magnetic field, the magnetic loss is high [43]. This study used flexible magnetic material cores comprising an insert block with low loss and high permeability ($\approx$ 230) [44], [45], where the flexibility improves system robustness against mechanical stress and vibration [46]. The cores are made of liquid silicon rubber with a magnetic filler in form of a powder and cut by laser to fixes custom request designs in the realistic manufacture [47]. The characteristic of this material and its fabrication makes it possible to match shapes of many sizes and take any desired form.

C. ASSESSMENT OF HUMAN PROTECTION FROM WPT SYSTEMS IN EVS

As ensuring human protection is of utmost importance when implementing WPT systems in EVs, numerous studies have been conducted to explore this topic, shedding light on different aspects of human protection. For instance, De Santis et al. [48] and Miwa et al. [49] performed dosimetry analysis for carbon fiber-reinforced plastic EVs. Meanwhile, ferrite cores [50] or metal plates [51] have been used as shielding to reduce magnetic field density values, which were investigated and measured in terms of human exposure. Furthermore, Cimala et al. [18] investigated the scenario of a human body exposed to an IPT system magnetic field in an EV or hybrid vehicle while considering the finite conductivity of the vehicle body. A previous study [52] defined safe, efficient, and intelligent complementary alternating current (AC) and direct current (DC) power sources as the basis for the safe operation of EV charging stations. These studies have underscored the need for comprehensive measures to mitigate potential risks and ensure effective protection ()()() [53]. In addition, several other related studies have contributed valuable insights into human safety with EV IPT systems. For instance, another study [54] proposed an optimization framework to minimize magnetic field exposure on humans using the concept of magnetic shielding. Another study [55] investigated the effects of different vehicle materials on magnetic field distribution and human exposure, providing valuable data for designing safer EV IPT systems. Moreover, previous research has evaluated induced electric fields produced by EV WPT systems using different human models [56], [57] and postures [58].

III. MODEL AND METHOD

First, the WPT system and its details are described. Then, a two-stage computational method used in this study is detailed [59]. In the first stage, full-wave electromagnetic simulation has been performed for the magnetic field distribution (Sec. III-E). In the second stage, the induced electric field is computed using the quasi-static dosimetry method (Sec. III-F). The proposed computational approach has been validated by intercomparison with [60] and [61].

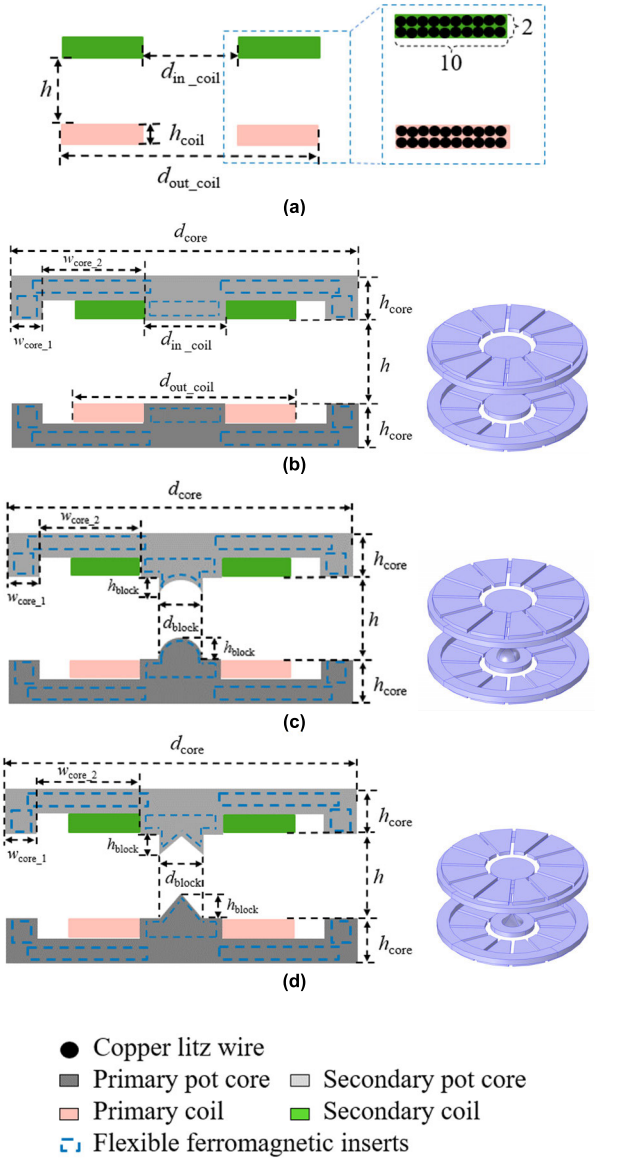

FIGURE 1. Geometry structure of the four wireless power transfer (WPT) systems and their insert structures (cross-section, unit: mm): (a) core-less, (b) core-based I, (c) core-based II, and (d) core-based III.

A. GEOMETIC STRUCTURE OF THE PROPOSED WPT SYSTEM

As shown in Fig. 1, the WPT system includes transmitting and receiving coils with identical structures. Each comprises a double-layer coil made of Φ 4.6-mm copper litz wires with 20 (10 $\times$ 2) turns. The coils using litz wires can achieve high efficiency that can help mitigate skin and proximity effects,

thereby minimizing losses owing to eddy AC currents [62]. Moreover, the double-layer structure of the coil has been used in many of the EV-WPT system [63], [64].

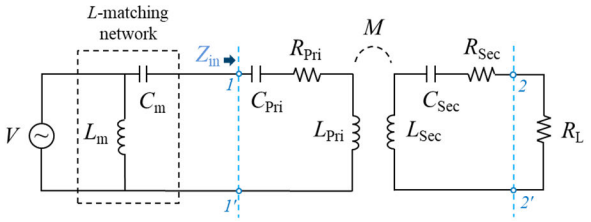

FIGURE 2. Equivalent circuit of the WPT system with the matching circuit ($R_{in} < R_0$).

In this study, the transmitting and receiving coils form a ''core-less'' system, as shown in Fig. 1(a). The inner diameter of the coil is set to $d_{\text{in\_coil}} = 82$ mm, and the outer diameter is set to $d_{\text{out\_coil}} = 174$ mm. Also, when the coil is tightly wound, the minimum channel width of adjacent wires is zero. Moreover, the primary and secondary coils are initially separated by a distance of $h = 100$ mm, corresponding to the typical vehicle chassis height [65]. Fig. 2 displays the equivalent circuit of a typical inductive coupling WPT system. The system operational frequency is 85 kHz, which is in accordance with the EV wireless charging standard [16].

In this study, the field-circuit co-simulation method was used to evaluate the proposed WPT system transfer efficiency using the commercial software COMSOL Multiphysics 6.0 [66], [67]. As shown in Fig. 2, the power source can be modeled as a voltage source with internal resistance R_0 based on the Davidinan's theorem [68]. The transmitting and receiving coils in the system are characterized by internal resistance $R_{\text{Pri/Sec}}$ and self-inductances $L_{\text{Pri/Sec}}$ [69]. Furthermore, $R_{\text{Pri/Sec}}$ represents the ohmic losses of the coils. $L_{\text{Pri/Sec}}$ and $R_{\text{Pri/Sec}}$ are calculated using the frequency domain solver of the full-wave electromagnetic simulation package. The mutual inductance between the two coils is denoted as M, which connects the transmitter and receiver. The load resistance is set to 5 Ω [25]. Capacitors $C_{\text{Pri/Sec}}$ are introduced to resonate the transmitter and receiver at the desired frequency f_0, contributing to improved transfer efficiency [70]. $C_{\text{Pri/Sec}}$ is calculated as follows [71]:

$$C_{\text{Pri/Sec}} = \frac{1}{\omega_0^2 L_{Pri/Sec}} \tag{1}$$

where $\omega_0 = 2\pi f_0$, and $L_{\text{Pri/Sec}}$ is directly calculated using COMSOL.

In addition, one of the main challenges for WPT systems is to achieve an adequate level of power transfer efficiency as the distance between the transmitter and receiver varies. The L-shaped matching network, as the simplest network matching structure, is always used to overcome the mismatch problem [62]. As shown in Fig. 2, an arbitrary complex load at port 1–1' ($Z_{in} = R_{in} + jX_{in}$) can be matched to the characteristic impedance R_0 (shown in Eq. 2) by adjusting the parallel inductance L_{m} and the series capacitor C_{m} of matching network to achieve the maximum wireless power transfer efficiency.

$$\frac{1}{R_0} = j\frac{1}{\omega_0 L_m} + \frac{1}{R_{in} + jX_{in} + 1/j\omega_0 C_m} \tag{2}$$

The whole transfer efficiency η of the WPT system can be calculated can be expressed as follows:

$$\eta = \frac{P_{R_L}}{P_{in}} \tag{3}$$

where P_{in} and P_{R_L} are the input power (at port 1–1') and load power (at port 2–2'), respectively. In practical applications, the system is more intricate, and other components are in [72].

TABLE 1. Size values of the WPT system (unit: mm).

d_{core}	d_{block}	$d_{\text{in\_coil}}$	$d_{\text{out\_coil}}$	$w_{\text{core\_1}}$
270	41	82	174	5.5
h_{core}	h_{block}	h	h_{coil}	$w_{\text{core\_2}}$
20	20.5	100	9.2	70.4

TABLE 2. Electromagnetic properties of the different material using in simulation.

Parameter	Relative Permittivity	Relative Permeability	Electrical Conductivity [S/m]
Coil	1	1	5.998×10^{7}
Core	2.8	9.5	5×10^{-13}
Insert	6.9	230	5×10^{-5}

B. CORE-BASED WPT SYSTEM

As summarized in Section II-A, the pot core (core-based I), as shown in Fig. 1 (b), was simulated and evaluated herein. Litz wires were used for fabricating transmitting and receiving coils, similar to those in the core-less system. The pot core shield is placed over the transmitting/receiving coils to reduce unwanted magnetic leakages [73]. To improve the mutual coefficient between the coils and divert magnetic flux lines from potential victims, flexible ferrite sheets were used as inserts and then embedded in the primary and secondary pot cores [47], [74]. The insert parts match the slots of the pot structures. In addition, the inserts can effectively improve the transfer efficiency [43]. The pot core and coils formed the primary and secondary parts of the system, respectively, and were of equal size [16]. The size of the cores was determined based on their geometry, as introduced in Section III-A. To symmetrically and tightly settle the coils on the core surface,

the core height is set to $h_{\text{core}} = 14.4$ mm. The protrusion with a width of $w_{\text{core\_1}} = 5.5$ mm on the outside of each core constrains the leakage field outside the coil and serves to collect the field and reduce leakage. For the core to cover the entire surface of the coils, the core notch width $w_{\text{core\_2}}$ should be larger than the ring widths of the coils (($d_{\text{out\_coil}}$ - $d_{\text{in\_coil}}$)/2) and equal to 70.4 mm. Also, the core diameter is larger than the outer diameter of the coils and is set to $d_{\text{core}} = 270$ mm.

Figs. 1 (b) and (c) depicts the core-based II and III systems, respectively, showcasing their distinct center components compared to the core-based I system. The secondary part of the core-based II system incorporates a hemispherical intermediate block, whereas the corresponding primary part has a hemispherical void. Similarly, the secondary part of the core-based III system uses a conical intermediate block, whereas the corresponding primary part has a conical void. The intermediate block diameter is set to $d_{\text{block}} = 41$ mm ($= d_{\text{in\_coil}}/2$). The intermediate block height is set to $h_{\text{block}} = 20.5$ mm, which is the same as the intermediate block radius ($d_{\text{block}}/2$). These complementary intermediate blocks are designed to alter the direction of magnetic flux lines. Also, using these specific geometric shapes, the core-based II and III systems aim at reducing magnetic field leakage and improving system performance. In addition, the system misalignment condition is also considered, as the scenario could possibly result in leaked magnetic field strength, corresponding to the worst-case exposure. The power loss in each proposed core has been computed as shown in Fig. 3. The transferred power is set to 1 kW and the transmission distance to 100 mm.

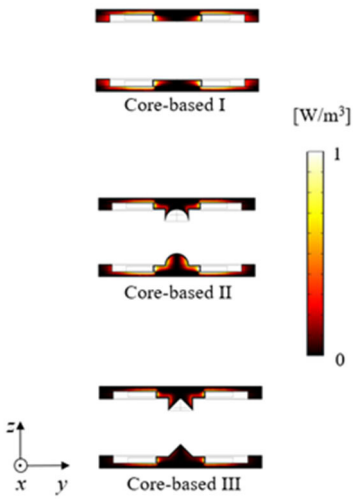

FIGURE 3. Power loss in each core of the 3 core-based WPT systems.

Table 1 summarizes the geometrical parameters of the four WPT systems. Moreover, Table 2 lists their electromagnetic parameters. The relative permittivity, relative permeability, and electrical conductivity with respect to the core along with the insert material were measured at the LVSP Institute of Polymer Materials, Friedrich-Alexander-Universität Erlangen-Nürnberg (FAU) [44], [45]. In [41], the detailed production process of the core material is explained. From the paper, the hysteresis curves of the core material show almost perfect linear relation up to 9000 A/m at 50 Hz. In addition, the effectiveness of the material at 100 kHz is also shown at least up to 4000 A/m [41]. The computational results shown below will be within this range.

C. VEHICLE CABIN MODEL

A simplified vehicle cabin model based on the Toyota Motor Corporation Prius [49], for which the WPT system is implemented, is depicted in Fig. 4 (a). The vehicle body is assumed to be placed in free space. As the relative permeability of a window is 1, glass windows in the vehicle were not considered in the evaluation because of their negligible impact on the magnetic field [67]. The vehicle body is fabricated using aluminum with 2.0 mm thickness.

D. HUMAN BODY MODEL

For a realistic assessment of exposure dose, the Japanese adult male human body model, TARO [75], was used in this study (Fig. 4 (b)). This voxel-based model includes 51 tissues/organs, with a spatial resolution of 2 mm. The dielectric properties of the tissues were determined using the four-Cole–Cole dispersion model [76].

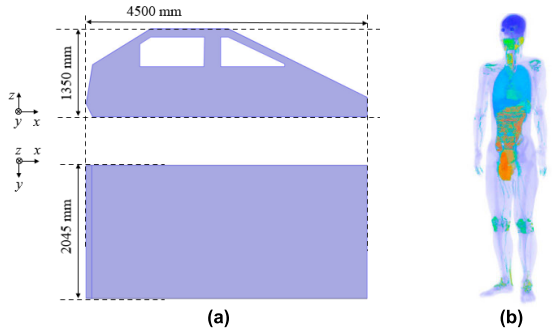

FIGURE 4. (a) Cross-section of the electric vehicle (EV) cabin model (xz-plane and xy-plane) and (b) Japanese adult male model TARO.

E. SIMULATION FOR MAGNETIC FIELD

Based on the method in Section III-A, this study evaluated the transfer efficiency and magnetic field distribution of the proposed WPT system. The simulation domain was defined as a sphere with a radius of 2.5 m. Tetrahedral meshes were used to discretize the simulation domain, with the mesh sizes automatically determined by the COMSOL software. Without changing any parameters, COMSOL produces consistent results for every calculation. The impact of using finer settings was also tested and unaffected by the applied discretization resolution ($< 1\%$). Meanwhile, the perfectly matched layer was used to truncate the computational region.

The values of matching circuits L_m and C_m were calculated based on input and load resistances [68]. For the core-based I–III systems at the transmission distance $h = 100$ mm, $C_m = 22.1$, 25.7, and 26.4 μF, $L_m = 26.6$, 28.1, and 28.1 μH, respectively. By using the matching network, the power conversion efficiency of each system is 99.7%, 99.8%, and 99.8%, respectively.

As shown in Fig. 5(a) [55], [67], the WPT system is installed below the vehicle body center with the receiving coil positioned at the end closest to the car chassis. At a transmission distance of 100 mm, the magnetic field distribution for each system with and without the vehicle model was initially compared with the perfectly aligned coils. Then, the effect of misalignment on the system with the vehicle model has been studied where the offset is set to Δy along the y-axis, positive direction.

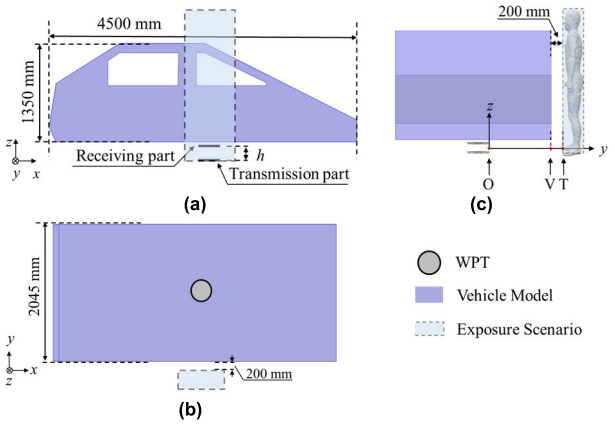

FIGURE 5. WPT location with respect to the vehicle cabin and TARO model: (a) xz-plane (b) xy-plane and (c) yz-plane. In Fig 5 (c), the point O represents the core-based system edge; point V represents the vehicle model location edge; and point T represents the start of the TARO model exposure scenario.

F. SIMULATION OF EXPOSURE DOSES IN THE TARO MODEL

A realistic anatomical human body model (TARO) was used to evaluate the induced electric field generated by stray magnetic fields using the proposed WPT systems. The magneto-quasi-static approximation can be used to compute the induced electric field when the frequency is lower than 10 MHz [59], [77].

Stray magnetic fields around the system and vehicle model were simulated using the FEM in the presence of the vehicle model. The resulting magnetic vector potential values were then calculated using COMSOL. Next, an in-house-developed solver created by Nagoya Institute of Technology (NITECH) based on the SPFD method was used to compute the induced electric field using the magnetic vector potential values serving as the source for computation [78]. This code has been validated via international intercomparison study [79]. This represented exposure to the external WPT magnetic field, wherein the presence of the human body model did not retroact on the external magnetic field distribution [26]. In addition, at low frequencies, the displacement current could be disregarded. This approach involves discretizing the computational target with cubical voxels and creating simultaneous linear equations for all contacts with the electric scalar potential serving as the unknown variable. The internal electric field is derived through matrix calculations, and the resulting matrix equation is solved using the geometric multigrid method.

G. EXPOSURE SCENARIO

The light-blue rectangular shown in Fig. 5 illustrates the exposure scenario in this study, where TARO was placed near the center of the vehicle with its lowermost point (feet) aligned with the horizontal position of the system transmitting coil. The front-facing aspect of TARO was directed toward the vehicle model while maintaining a separation distance of 200 mm [80]. All computational analyses were performed with respect to a constant power transfer of 1 kW at 85 kHz. For post-processing, the induced electric field of a 2 mm cube was evaluated, which is a metric described in the International Commission on Non-Ionizing Radiation Protection (ICNIRP) guidelines [20].

IV. RESULTS

A. WPT SYSTEM PERFORMANCE

This study evaluates the transmission efficiency of WPT systems over different transmission distances, ranging from 100 to 300 mm. For fundamental discussion, the vehicle body is not considered herein. As shown in Fig. 6 (a), the transmission efficiency of all types of WPT systems decreased with increasing transmission distance h. The results also showed that the WPT systems using ferrite cores exhibit better transmission efficiency than the core-less WPT system.

The difference between the transmission efficiencies of the two systems increased with transmission distance. When the transmission distance is 300 mm, the transfer efficiency of the core-based systems reaches the maximum that is 34% higher than that of the core-less system. Meanwhile, a 4% increase in maximum for transmission efficiency is observed in the core-based II and III systems compared to the core-based I system. Nevertheless, the core-based II and III systems exhibited nearly identical transmission efficiencies despite having different intermediate blocks.

Considering the misalignment condition, Fig. 6 (b) shows the results of the four system. Meanwhile, transmission distance is set to $h = 100$ mm and the offset of the primary part Δy is set from 0 to 250 mm, positive direction through the y-axis. As the misalignment distance widens, the core-less system transfer efficiency initially decreases and then temporarily increases. Considering the core-based system, it can be observed that a ‘‘valley’’ exists in the proposed coil array

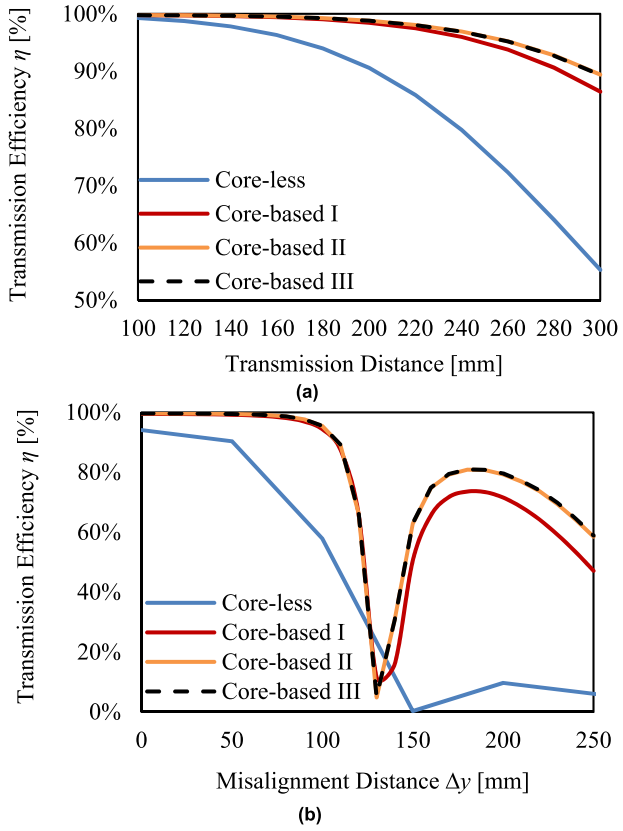

FIGURE 6. Transmission efficiency of four WPT systems variation with (a) transmission distance h and (b) misalignment distance Δy.

between 120 to 180 mm. At misalignment distances greater than 200 mm, the core-based I system transmission efficiency is 5% lower than that of the core-based II and III systems.

B. MAGNETIC FIELD DISTRIBUTION

Herein, the magnetic field distributions of the four WPT systems are compared without considering the vehicle model. The results shown in Fig. 7 indicate that the magnetic field distribution produced by the core-less WPT system has a wider range than that of the core-based systems. The core-less WPT system moderately exhibited strong magnetic field strength at the front and back sides of each coil. However, magnetic flux in the core-based systems is guided by the high magnetic permeability of the two cores, resulting in a substantial increase of magnetic field intensity between the two coils. In the three core-based WPT systems, the magnetic flux at the rear of the coils is restricted, indicating that the added core acts as a shield. Compared with the core-based I system, changes in the structural composition of the center part of the core-based II and III systems increase magnetic field intensity in the central region of the systems and the convergence of the external magnetic field range.

Fig. 8 illustrates the magnetic field distribution of the four WPT systems in the presence of the vehicle model while the coils are perfectly aligned. The core-less WPT system

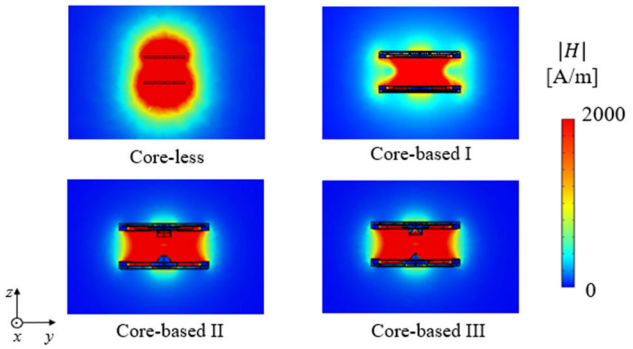

FIGURE 7. Magnetic field distribution (*H* [A/m]) for the cross-section of the perfectly aligned WPT models. The transferred power was set to 1 kW.

produced the widest magnetic field distribution range underneath the vehicle model. Furthermore, the presence of cores in the core-based WPT systems reduced the magnetic field leakage range, with the core-based II and III systems exhibiting a smaller leakage range than the core-based I system.

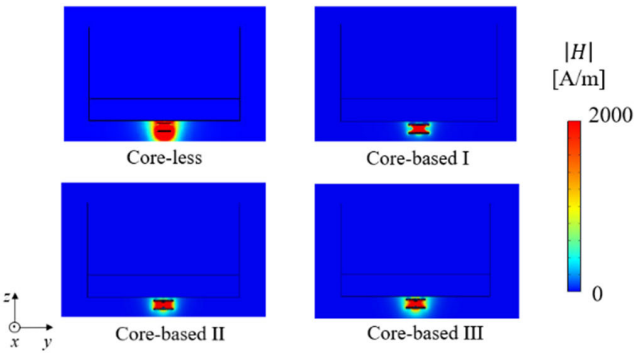

FIGURE 8. Magnetic field distribution (*H* [A/m]) for the cross-section of the perfectly aligned WPT models with the vehicle model. The transferred power was set to 1 kW.

Fig. 9 shows the magnetic field strength of each system along the *y*-axis from point O as the coordinate origin (Fig. 5 (b)) to the outside of the system while the transmission part and the receiving part are perfectly aligned. The results show that the magnetic field strength decreases gradually increasing the distance from the system, regardless of the presence or absence of the vehicle model. When only considering the system, the external magnetic field strength is initially nearly identical. However, as distance from the system increases, the magnetic field strength values with respect to the core-less and core-based I systems remain relatively consistent and higher than those with respect to the core-based II and III systems. The external magnetic field strength of the core-based II is marginally higher than that of the III system. Compared with the core-less and core-based I systems, the core-based II and III systems can reduce the external magnetic field intensity by 77.4% and 81.9% at point T, respectively. Although the core-based II and III systems have intermediate blocks, the magnetic field

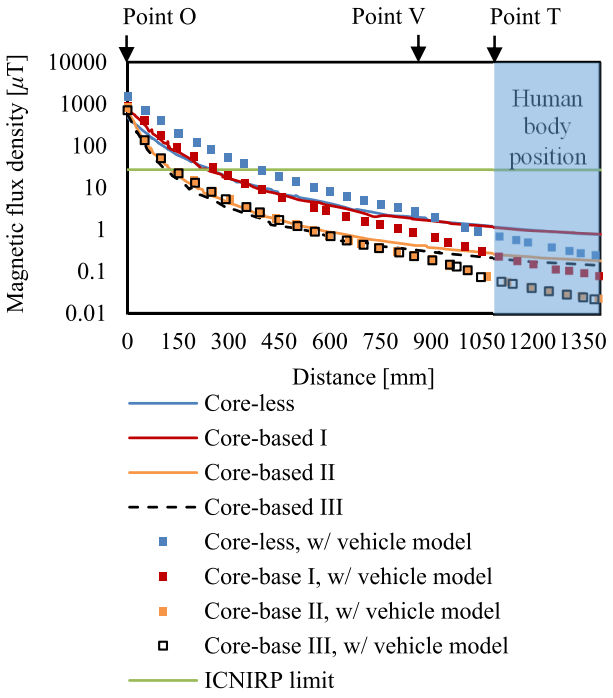

FIGURE 9. Comparison of the external magnetic flux density of four WPT systems with the limit of ICNIRP guidelines.

intensity of the core-based III system is lower than that of the core-based II system, demonstrating that modifications in the intermediate block structure can reduce magnetic field leakage.

As depicted in the figure, the core-less system external magnetic field strength remains consistently higher than that of the other three core-based systems when considering the system with the vehicle model. Comparing the external magnetic field strength of the three core-based systems, core-based I exhibits higher values than the nearly identical values of core-based II and III. Comparatively, the core-based I–III systems can reduce the external magnetic field strength by a maximum of 64.8%, 91.5%, and 91.6%, respectively, compared with the core-less system at point T. According to the ICNIRP 2010 guidelines, the magnetic field limit for 3–100 kHz is 27 μT for public exposure. Following the magnetic field limit of ICNIRP, the maximum permissible transferred power of the core-less and core-based I–III systems is 36, 108, 450, and 450 kW, respectively.

The magnetic field distribution of the three core-based systems were also studied with the misalignment condition. It was found that the misaligned distance Δy corresponds to a transfer efficiency of 95% in each core-based system [22]. Fig. 10 illustrates the magnetic field distribution of the three core-based WPT systems, in the presence of the vehicle model. The value of Δy with core-based I–III systems is 96, 100, and 100 mm, respectively. As can be observed, the misalignment condition leads to an increase in the magnetic field strength.

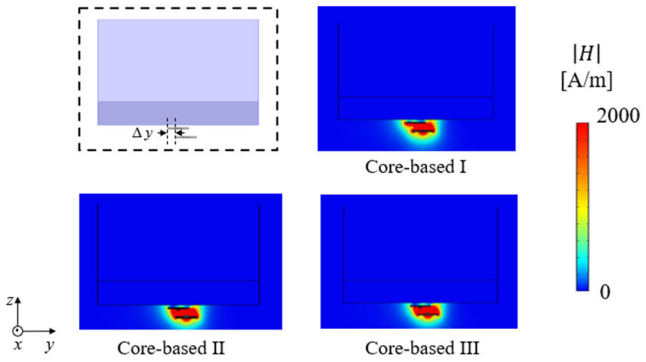

FIGURE 10. Magnetic field distribution (H [A/m]) on the misaligned WPT models with the vehicle cabin model cross-section.

The transferred power was set to 1 kW and the misalignment distance Δy corresponds to a transfer efficiency of 95%. Considering the perfectly aligned and misaligned conditions, Fig. 11 shows the magnetic field strength of each core-based system along the y-axis from point O. The results show that magnetic field strength decreases gradually with increasing distance, observing nearly identical values for all three systems. The core-based I–III systems at the misalignment condition increased the external magnetic field strength by 81.5%, 93.3%, and 93.3%, respectively, compared with the perfectly aligned condition at point T. Following the magnetic field reference level of ICNIRP, the maximum permissible transferred power of the core-based I–III systems was 20, 24.3, and 24.3 kW, respectively.

C. INDUCED ELECTRIC FIELD

Fig. 5 illustrates the WPT locations relative to TARO, where the distance in considering the vehicle model is set to 200 mm [80]. The simulation results, as shown in Fig. 12 for the aligned and misaligned coil position, revealed that the WPT system with a core structure reduced the distribution and strength of the induced electric field in the TARO model. In all four perfectly aligned systems, being the parts of the body closest to the vehicle, hotspots appeared around the feet/lower legs, calves, and between the legs of TARO. However, when considering the three core-based systems at the misalignment condition, hotspots appeared around the upper body. Furthermore, the WPT system with a core structure effectively reduced the intensity and spatial distribution of the electric field induced within the human body model. The WPT system core structure effectiveness varies, with the core-based II and III designs exhibiting greater reductions than the core-based I design in the induced electric field.

Table 3 lists the maximum induced electric field strength averaged over a 2 mm cube within the TARO model for the four WPT systems, with evaluations made for the perfectly aligned and misaligned cases. The results demonstrate superior performance by the three core-based WPT systems over the core-less WPT system in terms of reducing the induced electric field strength. Meanwhile, when considering the four

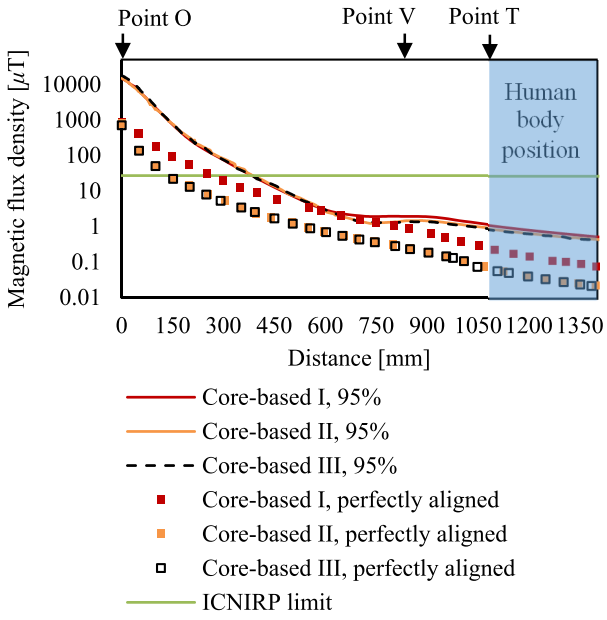

FIGURE 11. Comparison of the external magnetic flux density of three core-based WPT systems for the perfectly aligned and misaligned conditions with the limit of ICNIRP.

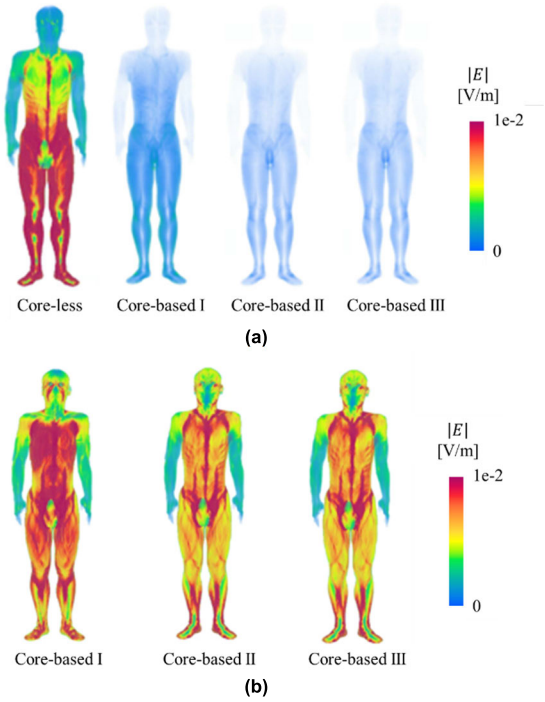

FIGURE 12. Distributions of induced electric field strength on the TARO model body surface (a) nearby the perfectly aligned system and (b) nearby the misalignment system.

systems at the perfectly aligned case, the core-based I–III systems exhibit reductions of 93.6%, 90.5%, and 98.3%, respectively, in the induced electric field strength compared with the core-less system. This reduction is primarily attributed to the core structure, which effectively suppresses electromagnetic field leakage around the WPT system.

Our computational value with 1 kW is scalable multiplying the induced electric field by multiply the ratio of the target transmitted power (kW value) to 1 kW. Considering the transferred power at 11 kW for the perfectly aligned case, the maximum induced electric field strength in this exposure scenario is 1.82 V/m for core-less, 0.11 V/m for core-based I, 0.03 V/m for core-based II and core-based III. According to the ICNIRP 2010 guidelines, the induced electric field limit is 11.48 V/m for public exposure; the induced electric field in the body caused by the four systems is below 1% of the basic restriction. Following this limit, the maximum permissible transferred power of the core-less and core-based I–III systems was 69.6, 1.1×10^3, 3.67×10^3, and 4.05×10^3 kW, respectively.

TABLE 3. Maximum values of the induced electric field strength (unit: mV/m), the misalignment distance corresponds to a transfer efficiency of 95%.

Case	Core-less	Core-based I	Core-based II	Core-based III
Perfectly aligned	165	10.4	3.13	2.83
Misaligned	N/A	66.2	55.7	55.6

Considering the transferred power at 11 kW in the misalignment condition, the maximum induced electric field strength in this exposure scenario is 0.72 V/m for core-based I, 0.61 V/m for core-based II and core-based III. The induced electric field in the body caused by the three misaligned systems is below 1% of the basic restriction. Following the ICNIRP limit, the maximum permissible transferred power of the core-based I–III systems was 173, 206, and 207 kW, respectively.

V. DISCUSSION

This study evaluated one core-less and three core-based WPT systems used for charging EVs. The evaluation criteria for these systems included transmission efficiency, leaked magnetic field intensity, and induced electric field in the anatomical human model placed near the vehicle. Moreover, this study considers two positional cases: perfectly aligned and misaligned.

Computational results obtained from full-wave simulations demonstrated that for the perfectly aligned case the transmission efficiency of these WPT systems decreased with increasing transmission distance, without considering the vehicle body model. This reduction in efficiency can be primarily attributed to the decrease in the coupling coefficient [81]. Furthermore, the core-based systems exhibited higher transmission efficiency than the core-less system. This is because the ferrite core in core-based systems can greatly divert magnetic flux lines, resulting in magnetic field concentration around the coils (Fig. 7) [45]. Moreover, the

TABLE 4. Comparison of the related research.

Year	2013 [56]	2015 [22]	2017 [35]	2018 [43]	2018 [48]	2018 [50]	2019 [83]	This study
Shield type	Rectangular core	N/A	Ferrite core + Aluminum plate	Ferromagnetic core + Aluminum plate	N/A	Ferrites tiles + Metal plate	Ferrite core + Aluminum shielding plate	Pot core + Magnetic material insert block
Operating Frequency	85 [kHz]	85 [kHz]	85 [kHz]	85 [kHz]	85 [kHz]	125 [kHz]	85 [kHz]	85 [kHz]
Max. Tx diameter /Length [mm]	405	405	600	600	500	600	500	270
Air gap [mm]	150	120	150	200	200	200	150	100
Transferred power [kW]	7	7	5	3.5	7.7	7.7	5	3.7
Efficiency at aligned case [%]	97.1	97.1	$k = 0.298$	96	$k = 0.07$	96	78	99.6
Magnetic field discussion	The averaged magnetic field strength that the model occupies is at most one half (adult models) or equal to (child) the reference level for the general public.	N/A	The magnetic flux density reduces by 25% for the optimized core configuration.	Reduced the magnetic flux density on the Rx core by about 44%.	Misalignment condition leads to an important increase of the magnetic field level.	The maximum magnetic field strength of the WPT system equipped with the ferrites was 28 A/m.	Reduced about 81% and 95% of the EMF average for the z-axis and x-axis, respectively.	Reduced the magnetic flux density on the human position up to 34%.
Human safety calculation	The maximal induced electric field in the body is at most 25% of the basic restriction.	The maximal induced electric field is 0.4 V/m.	N/A	N/A	Normalized to the peak value of induced electric field is 13.3 V/m for the aligned case; 19.9 V/m for misaligned case.	The maximal induced electric field is 0.42 V/m	N/A	The maximal induced electric field is 0.12 V/m
Considered exposure scenario	Human model is standing near to a vehicle model.	Human model is standing near to a vehicle model.			Human model inside the vehicle as driving passenger.	Human model is standing near the coil, human-coil distance is 235 mm.		Human model is standing near the vehicle, human-vehicle distance is 200 mm

incorporation of hemispherical and conical intermediate blocks enhanced the ability of the systems to divert flux lines and reshape the magnetic distribution. Hence, these blocks reduce unwanted emissions and increase transmission efficiencies of the core-based II and III systems that are higher than that of the core-based I system. Overall, the proposed core system exhibits good performance, with a transmission efficiency exceeding 89% at a coil distance of 300 mm despite the core diameter of 270 mm. These results indicate that the proposed core design has been adapted to the system, as reducing core size is a critical factor in improving system efficiency while maintaining high-power transfer capability [30]. In addition, previous research has also been compared with this study, as shown in Table 4.

A transmission efficiency of 95% is often used as a misalignment condition that accounts for the above losses and uncertainties in practical EV-WPT systems [22]. It provides a margin for variations in alignment, environmental conditions, and system imperfections, ensuring that the system can still effectively function even under less-than-optimal conditions. In studying the variation of transmission efficiency in the presence of misalignment, we found that the proposed system is sensitive to misalignment. The ''valley'' phenomenon is generally owing to the varying effects of magnetic flux cancellation at different lateral displacements coupled with changes in the coupling coefficient.

Considering the perfectly aligned condition, the external magnetic field distribution and strength of the core-based

systems were lower than the core-less system. The maximum magnetic field strength generated by the systems near the feet does not exceed the ICNIRP reference level, wherein the core-based systems achieved a maximum reduction of 91.6%, which is substantially lower than that of the core-less system. Hence, the induced electric field value generated by the external magnetic field in the TARO model is reduced by a maximum of 98.3%. These results indicate that the proposed core structure can reduce the adverse effects of EMFs generated by IPT systems on human health.

The magnetic field intensity range in the central region of the core-based II and III systems is enhanced compared to that of the core-based I system. This is because the direction of magnetic fluxes between the two coils is altered in the cases of systems II and III, causing external stray fluxes (especially around the core structures) to be substantially redirected toward the middle part of the system. Hence, the magnetic field strength between the coils increases, the magnetic field distribution range in the system central region expands, and the external magnetic field range converges, reducing magnetic field leakage. When considering the vehicle in studying the magnetic field distribution of the systems, structural changes in the center region of the core-based II and III systems altered the direction of magnetic fluxes toward the center of the system, reducing external magnetic field leakage. This finding is consistent with results related to the magnetic field distribution of the system without the vehicle model. Results in this study also reveal that the misalignment condition leads to the magnetic field level increase when compared to the perfectly aligned system. This finding is consistent with the observations in [48]. Moreover, core-based II and III shows more reduced this effect more than core-based I system for the misalignment condition.

Furthermore, even with similar magnetic field distributions and transmission efficiencies, the core-based III system exhibits greater reduction in external magnetic field strength and induced electric field value than the core-based II system, suggesting that core structure modifications can facilitate the design of safe WPT systems to improve safety during practical applications.

In the exposure scenario considered in this study, the maximum permissible transferred power calculated based on the ICNIRP limits of the induced electric field is 9.1 times higher than the maximum permissible transferred power calculated based on the magnetic field strength limits. This disparity highlights the importance of evaluating induced electric fields when calculating permissible power transfer, which is also highlighted in the intercomparison of [56]. Moreover, the result obtained herein agrees with the result presented in that study.

This study places a greater emphasis on exposure dose analysis for evaluating EMF protection issues compared to studies solely focused on system design, where the core materials utilized have been previously fabricated and validated, as referenced in Ref. [45], The ferromagnetic properties of these materials have been extensively discussed and experimentally confirmed in the same reference. Our study incorporates these materials, modifying only their size. Moreover, since the measurements of internal fields are impossible, numerical validation is commonly applied as mentioned by other related researches [17], [48], [53], [82]. In our previous study, for the coil without core have been validated for the simplified vehicle model before this study with using same computational approach [61], which is already mentioned in the Section III. The above rationale supports not providing experimental results in this time.

The core structure presented herein can minimize the overall system volume and streamline the installation process compared with other shielding devices using WPT systems for charging EVs [83]. The primary reason for the differences among the core-based systems I–III is the distinct design of the core center. Although modifying the core center can reduce adverse effects on human health, this modification increases the weight and cost of the systems.

While it is beyond the scope of this study to discuss how implantable devices are affected, Hikage et al. [84] mentioned that the observed characteristics of the maximum interference distance of implantable devices depend upon the magnetic field distribution close to resonant WPT antennas and coil size. In addition, previous studies founded that the use of different materials/models can affect the magnetic field distribution inside and outside the vehicle body [55], [85]. Moreover, although the problem with discharge at the sharp points didn't find in our study, this material/structure should be analyzed specifically when applied to high power transmission.

Despite the advantages of using IPT systems for charging EVs, some of its limitations need to be addressed in future research. For example, transmission distance may vary under different environmental conditions. Furthermore, considering the installation surroundings such as the possibility of uneven terrain or other equipment being simultaneously installed in the vehicle may affect the performance and safety of the system. A detector may also need to be considered in the system for animal protection from the application.

VI. CONCLUSION

In this study, three core structures with respect to efficient inductive WPT systems were considered to minimize magnetic field leakage. These core structures were evaluated against a core-less system in terms of efficiency without considering the vehicle model, leaked magnetic field strength with and without considering the vehicle model, and induced electric field strength. Scenarios considering perfectly aligned and misaligned condition have been discussed. By concentrating on the magnetic field within the core structure and reducing its diffusion outside the system, EMF exposure was effectively reduced. For compliance assessment, a common exposure scenario, in which a human model stands near an EV, was considered. Using the proposed core structures, the results revealed a substantial reduction in the exposure doses of up to 90% with respect to the

human body. The induced electric field within the body resulting from the proposed systems, under perfectly aligned and misaligned conditions, is below 1% of the basic restriction. Furthermore, the computation of this study showed that the proposed intermediate block within the core can further reduce magnetic field leakage and resultant adverse effects on the human body. This demonstrates the importance of designing a core structure with the aim of reducing EMF exposure from WPT systems to humans. However, the tradeoff between the improvements achieved and the associated increase in cost and weight owing to the core material used needs to be considered. Therefore, future research must focus on the proposed core structures for specific applications and consider the tradeoffs among efficiency, safety, cost, and weight. Experimental validation of the simulation results is also recommended to further improve the accuracy and reliability of the proposed WPT systems.

REFERENCES

[1] Y. Yang, M. El Baghdadi, Y. Lan, Y. Benomar, J. Van Mierlo, and O. Hegazy, "Design methodology, modeling, and comparative study of wireless power transfer systems for electric vehicles," *Energies*, vol. 11, no. 7, p. 1716, Jul. 2018, doi: 10.3390/en11071716.

[2] M. Scudiere and J. McKeever, "Wireless power transfer for electric vehicles," SAE Tech. Paper 2011-01-0354, 2011, doi: 10.1049/etr.2015.0017.

[3] Y. Jang and M. M. Jovanovic, "A contactless electrical energy transmission system for portable-telephone battery chargers," *IEEE Trans. Ind. Electron.*, vol. 50, no. 3, pp. 520–527, Jun. 2003, doi: 10.1109/TIE.2003.812472.

[4] M. Rasouli and L. S. J. Phee, "Energy sources and their development for application in medical devices," *Expert Rev. Med. Devices*, vol. 7, no. 5, pp. 693–709, Sep. 2010, doi: 10.1586/erd.10.20.

[5] V. Cirimele, M. Diana, F. Freschi, and M. Mitolo, "Inductive power transfer for automotive applications: State-of-the-art and future trends," *IEEE Trans. Ind. Appl.*, vol. 54, no. 5, pp. 4069–4079, Sep. 2018, doi: 10.1109/TIA.2018.2836098.

[6] T. Shijo, K. Ogawa, and S. Obayashi, "Optimization of thickness and shape of core block in resonator for 7 kW-class wireless power transfer system for PHEV/EV charging," in *Proc. IEEE Energy Convers. Congr. Expo. (ECCE)*, Sep. 2015, pp. 3099–3102, doi: 10.1109/ECCE.2015.7310094.

[7] J. Tritschler, S. Reichert, and B. Goeldi, "A practical investigation of a high power, bidirectional charging system for electric vehicles," in *Proc. 16th Eur. Conf. Power Electron. Appl.*, Aug. 2014, pp. 1–7, doi: 10.1109/EPE.2014.6910809.

[8] S. Obayashi et al., "85 kHz band 44 kW wireless rapid charging system for field test and public road operation of electric bus," *World Electr. Vehicle J.*, vol. 10, no. 2, 2019, Art. no. 26, doi: 10.3390/wevj10020026.

[9] E. Aydin, M. T. Aydemir, A. Aksoz, M. El Baghdadi, and O. Hegazy, "Inductive power transfer for electric vehicle charging applications: A comprehensive review," *Energies*, vol. 15, no. 14, p. 4962, Jul. 2022, doi: 10.3390/en15144962.

[10] *IEEE Standard for Safety Levels With Respect to Human Exposure to Electric, Magnetic, and Electromagnetic Fields, 0 Hz to 300 GHz Corrigenda 2*, Standard C95.1-2019/Cor2-2020 (Corrigenda to IEEE Std C95.1-2019), 2020, pp. 1–15, doi: 10.1109/IEEESTD.2020.9238523.

[11] International Commission on Non-Ionizing Radiation Protection, "Guidelines for limiting exposure to electromagnetic fields (100 kHz to 300 GHz)," *Health Phys.*, vol. 118, no. 5, pp. 483–524, 2020, doi: 10.1097/HP.0000000000001210.

[12] *Electric Vehicle Wireless Power Transfer (WPT) Systems—Part 1: General Requirements*, document IEC 61980-1, Int. Electrotech. Commun., 2020.

[13] *Electric Vehicle Wireless Power Transfer (WPT) Systems—Part. 2: Specific Requirements for Communication Between Electric Road Vehicle (EV) and Infrastructure*, document IEC 61980-2, Int. Electrotech. Commun., 2023.

[14] *Electric Vehicle Wireless Power Transfer (WPT) Systems—Part 3: Specific Requirements for the Magnetic Field Wireless Power Transfer Systems*, document IEC 61980-3, Int. Electrotech. Commun., 2019.

[15] A. Mahesh, B. Chokkalingam, and L. Mihet-Popa, "Inductive wireless power transfer charging for electric vehicles—A review," *IEEE Access*, vol. 9, pp. 137667–137713, 2021, doi: 10.1109/ACCESS.2021.3116678.

[16] *Wireless Power Transfer for Light-Duty Plug-in/Electric Vehicles and Alignment Methodology*, document SAE J2954:2022, 2022, p. 201, doi: 10.4271/J2954_202208.

[17] I. A. Shah and H. Yoo, "Assessing human exposure with medical implants to electromagnetic fields from a wireless power transmission system in an electric vehicle," *IEEE Trans. Electromagn. Compat.*, vol. 62, no. 2, pp. 338–345, Apr. 2020, doi: 10.1109/TEMC.2019.2903844.

[18] C. Cimala, M. Clemens, J. Streckert, and B. Schmuelling, "High-resolution magnetic-field exposure simulations of automotive inductive power-transfer systems using a scaled-frequency finite difference time domain approach with multi-GPU acceleration," *Int. J. Numer. Model., Electron. Netw., Devices Fields*, vol. 31, no. 2, pp. 1–5, Mar. 2018, doi: 10.1002/jnm.2231.

[19] W. Toshiaki and M. Ishida, "Study on the influence of the magnetic field and the induced electrical field in human bodies by EV/PHEV wireless charging systems," SAE Tech. Paper 2016-01-1158, 2016, p. 7, doi: 10.4271/2016-01-1158.

[20] International Commission on Non-Ionizing Radiation Protection, "Guidelines for limiting exposure to time-varying electric and magnetic fields (1 Hz to 100 kHz)," *Health Phys.*, vol. 99, no. 6, pp. 818–836, 2010, doi: 10.1097/HP.0b013e3181f06c86.

[21] G. Ziegelberger, "Gaps in knowledge relevant to the 'guidelines for limiting exposure to time-varying electric and magnetic fields (1 Hz-100 kHz)," *Health Phys.*, vol. 118, no. 5, pp. 533–542, 2020, doi: 10.1097/HP.0000000000001261.

[22] T. Shimamoto, I. Laakso, and A. Hirata, "Internal electric field in pregnant-woman model for wireless power transfer systems in electric vehicles," *Electron. Lett.*, vol. 51, no. 25, pp. 2136–2137, Dec. 2015, doi: 10.1049/el.2015.2457.

[23] P. S. R. Nayak, G. Peddanna, K. Kamalapathi, and B. K. Naick, "Analysis of mutual inductance between multi-single coupled coils at square structure using FEM," in *Proc. 1st Int. Conf. Electr., Control Instrum. Eng. (ICECIE)*, Nov. 2019, pp. 1–6, doi: 10.1109/ICECIE47765.2019.8974759.

[24] G. Ke, Q. Chen, L. Xu, S.-C. Wong, and C. K. Tse, "A model for coupling under coil misalignment for DD pads and circular pads of WPT system," in *Proc. IEEE Energy Convers. Congr. Expo. (ECCE)*, Sep. 2016, pp. 1–6, doi: 10.1109/ECCE.2016.7854706.

[25] X. Liu, C. Xia, and X. Yuan, "Study of the circular flat spiral coil structure effect on wireless power transfer system performance," *Energies*, vol. 11, no. 11, p. 2875, Oct. 2018, doi: 10.3390/en11112875.

[26] P. N. D. A. A. D. S. Pereira, R. D. S. G. Campilho, and A. M. G. Pinto, "Application of a design for excellence methodology for a wireless charger housing in underwater environments," *Machines*, vol. 10, no. 4, p. 232, Mar. 2022, doi: 10.3390/machines10040232.

[27] K. Aditya, "Analytical design of Archimedean spiral coils used in inductive power transfer for electric vehicles application," *Electr. Eng.*, vol. 100, no. 3, pp. 1819–1826, Sep. 2018, doi: 10.1007/s00202-017-0663-7.

[28] D. Kurschner, C. Rathge, and U. Jumar, "Design methodology for high efficient inductive power transfer systems with high coil positioning flexibility," *IEEE Trans. Ind. Electron.*, vol. 60, no. 1, pp. 372–381, Jan. 2013, doi: 10.1109/TIE.2011.2181134.

[29] T. Konstantinou, "Feasibility study and design of in-road electric vehicle charging technologies," Joint Transp. Res. Program Publication, Purdue Univ., West Lafayette, IN, USA, Tech. Rep. FHWA/IN/JTRP-2021/25, Oct. 2021, doi: 10.5703/1288284317353.

[30] G. A. Covic and J. T. Boys, "Modern trends in inductive power transfer for transportation applications," *IEEE J. Emerg. Sel. Topics Power Electron.*, vol. 1, no. 1, pp. 28–41, Mar. 2013, doi: 10.1109/JESTPE.2013.2264473.

[31] G. Elliott, S. Raabe, G. A. Covic, and J. T. Boys, "Multiphase pick-ups for large lateral tolerance contactless power-transfer systems," *IEEE Trans. Ind. Electron.*, vol. 57, no. 5, pp. 1590–1598, May 2010, doi: 10.1109/TIE.2009.2031184.

[32] M. Chigira, Y. Nagatsuka, Y. Kaneko, S. Abe, T. Yasuda, and A. Suzuki, "Small-size light-weight transformer with new core structure for contactless electric vehicle power transfer system," in *Proc. IEEE Energy Convers. Congr. Expo.*, Sep. 2011, pp. 260–266, doi: 10.1109/ECCE.2011.6063778.

[33] S. Kim, G. A. Covic, and J. T. Boys, "Tripolar pad for inductive power transfer systems for EV charging," *IEEE Trans. Power Electron.*, vol. 32, no. 7, pp. 5045–5057, Jul. 2017, doi: 10.1109/TPEL.2016.2606893.

[34] T. Kojiya, F. Sato, H. Matsuki, and T. Sato, "Automatic power supply system to underwater vehicles utilizing non-contacting technology," in *Proc. Oceans MTS/IEEE Techno-Ocean*, Nov. 2004, p. 2341, doi: 10.1109/OCEANS.2004.1406521.

[35] M. Mohammad, S. Choi, Z. Islam, S. Kwak, and J. Baek, "Core design and optimization for better misalignment tolerance and higher range of wireless charging of PHEV," *IEEE Trans. Transport. Electrific.*, vol. 3, no. 2, pp. 445–453, Jun. 2017, doi: 10.1109/TTE.2017.2663662.

[36] R. Haldi, K. Schenk, I. Nam, and E. Santi, "Finite-element-simulation-assisted optimized design of an asymmetrical high-power inductive coupler with a large air gap for EV charging," in *Proc. IEEE Energy Convers. Congr. Expo.*, Sep. 2013, pp. 3635–3642, doi: 10.1109/ECCE.2013.6647180.

[37] Z. Zhang, S. Zheng, Z. Yao, D. Xu, P. T. Krein, and H. Ma, "A coil positioning method integrated with an orthogonal decoupled transformer for inductive power transfer systems," *IEEE Trans. Power Electron.*, vol. 37, no. 8, pp. 9983–9998, Aug. 2022, doi: 10.1109/TPEL.2022.3155270.

[38] J. S. Choi, S. Y. Jeong, B. G. Choi, S.-T. Ryu, C. T. Rim, and Y.-S. Kim, "Air-gap-insensitive IPT pad with ferromagnetic and conductive plates," *IEEE Trans. Power Electron.*, vol. 35, no. 8, pp. 7863–7872, Aug. 2020, doi: 10.1109/TPEL.2019.2962194.

[39] N. E. Kazantseva, J. Vilčáková, V. Křesálek, P. Sàha, I. Sapurina, and J. Stejskal, "Magnetic behaviour of composites containing polyaniline-coated manganese-zinc ferrite," *J. Magn. Magn. Mater.*, vol. 269, no. 1, pp. 30–37, 2004, doi: 10.1016/S0304-8853(03)00557-2.

[40] Y. Bu, S. Endo, and T. Mizuno, "Improvement in the transmission efficiency of EV wireless power transfer system using a magnetoplated aluminum pipe," *IEEE Trans. Magn.*, vol. 54, no. 11, pp. 1–5, Nov. 2018, doi: 10.1109/TMAG.2018.2840109.

[41] M. Xiong, X. Wei, Y. Huang, Z. Luo, and H. Dai, "Research on novel flexible high-saturation nanocrystalline cores for wireless charging systems of electric vehicles," *IEEE Trans. Ind. Electron.*, vol. 68, no. 9, pp. 8310–8320, Sep. 2021, doi: 10.1109/TIE.2020.3016259.

[42] D. Barth, G. Cortese, and T. Leibfried, "Evaluation of soft magnetic composites for inductive wireless power transfer," in *Proc. IEEE PELS Workshop Emerg. Technol., Wireless Power Transf. (WoW)*, Jun. 2019, pp. 7–10, doi: 10.1109/WoW45936.2019.9030664.

[43] K. Elnail, X. Huang, C. Xiao, L. Tan, and X. Haozhe, "Core structure and electromagnetic field evaluation in WPT systems for charging electric vehicles," *Energies*, vol. 11, no. 7, p. 1734, Jul. 2018, doi: 10.3390/en11071734.

[44] D. W. Schubert, S. Werner, I. Hahn, and V. Solovieva, "Effect of particle size and size distribution on the permeability of soft magnetic liquid silicone rubber composites," *Compos. Sci. Technol.*, vol. 177, pp. 26–33, Jun. 2019, doi: 10.1016/j.compscitech.2019.04.005.

[45] H. F. Khalili, J. Kirchner, M. Bartunik, S. Werner, N. Ebel, D. W. Schubert, M. Weyand, and G. Fischer, "Transcutaneous energy transfer system for cardiac-assist devices by use of inhomogeneous biocompatible core material," *IEEE Trans. Magn.*, vol. 57, no. 12, pp. 1–12, Dec. 2021, doi: 10.1109/TMAG.2021.3119235.

[46] D. Patil, M. K. McDonough, J. M. Miller, B. Fahimi, and P. T. Balsara, "Wireless power transfer for vehicular applications: Overview and challenges," *IEEE Trans. Transport. Electrific.*, vol. 4, no. 1, pp. 3–37, Mar. 2018, doi: 10.1109/TTE.2017.2780627.

[47] *Würth WE-FSFS Flexible Sintered Ferrite Sheet*. Accessed: Nov. 23, 2023. [Online]. Available: https://uk.farnell.com/wefsfs-ferrite-sheet

[48] V. De Santis, T. Campi, S. Cruciani, I. Laakso, and M. Feliziani, "Assessment of the induced electric fields in a carbon-fiber electrical vehicle equipped with a wireless power transfer system," *Energies*, vol. 11, no. 3, p. 684, Mar. 2018, doi: 10.3390/en11030684.

[49] K. Miwa, T. Takenaka, and A. Hirata, "Dosimetry and compliance for wireless power transfer systems in vehicle," in *Proc. Int. Symp. Electromagn. Compat. EMC Eur.*, Sep. 2020, pp. 1–4, doi: 10.1109/EMCEUROPE48519.2020.9245849.

[50] J. Chakarothai, K. Wake, T. Arima, S. Watanabe, and T. Uno, "Exposure evaluation of an actual wireless power transfer system for an electric vehicle with near-field measurement," *IEEE Trans. Microw. Theory Techn.*, vol. 66, no. 3, pp. 1543–1552, Mar. 2018, doi: 10.1109/TMTT.2017.2748949.

[51] M. Budhia, G. A. Covic, and J. T. Boys, "Design and optimization of circular magnetic structures for lumped inductive power transfer systems," *IEEE Trans. Power Electron.*, vol. 26, no. 11, pp. 3096–3108, Nov. 2011, doi: 10.1109/TPEL.2011.2143730.

[52] F. Sanchez-Sutil, J. C. Hernández, and C. Tobajas, "Overview of electrical protection requirements for integration of a smart DC node with bidirectional electric vehicle charging stations into existing AC and DC railway grids," *Electric Power Syst. Res.*, vol. 122, pp. 104–118, May 2015, doi: 10.1016/j.epsr.2015.01.003.

[53] T. Campi, S. Cruciani, F. Maradei, and M. Feliziani, "Magnetic field during wireless charging in an electric vehicle according to standard SAE J2954," *Energies*, vol. 12, no. 9, p. 1795, May 2019, doi: 10.3390/en12091795.

[54] G. Talluri, M. Bindi, A. Luchetta, F. Grasso, L. Luchetti, and L. Paolucci, "Analysis of power losses due to magnetic shielding for electric vehicle wireless charging," in *Proc. IEEE 15th Int. Conf. Compat., Power Electron. Power Eng. (CPE-POWERENG)*, Jul. 2021, pp. 1–6, doi: 10.1109/CPE-POWERENG50821.2021.9501223.

[55] K. Miwa, T. Takenaka, and A. Hirata, "Electromagnetic dosimetry and compliance for wireless power transfer systems in vehicles," *IEEE Trans. Electromagn. Compat.*, vol. 61, no. 6, pp. 2024–2030, Dec. 2019, doi: 10.1109/TEMC.2019.2949983.

[56] I. Laakso and A. Hirata, "Evaluation of the induced electric field and compliance procedure for a wireless power transfer system in an electrical vehicle," *Phys. Med. Biol.*, vol. 58, no. 21, pp. 7583–7593, Nov. 2013, doi: 10.1088/0031-9155/58/21/7583.

[57] I. Laakso, T. Shimamoto, A. Hirata, and M. Feliziani, "Quasistatic approximation for exposure assessment of wireless power transfer," *IEICE Trans. Commun.*, vol. E98.B, no. 7, pp. 1156–1163, 2015, doi: 10.1587/transcom.E98.B.1156.

[58] T. Shimamoto, I. Laakso, and A. Hirata, "In-situelectric field in human body model in different postures for wireless power transfer system in an electrical vehicle," *Phys. Med. Biol.*, vol. 60, no. 1, pp. 163–173, Jan. 2015, doi: 10.1088/0031-9155/60/1/163.

[59] A. Hirata, F. Ito, and I. Laakso, "Confirmation of quasi-static approximation in SAR evaluation for a wireless power transfer system," *Phys. Med. Biol.*, vol. 58, no. 17, pp. N241–N249, Sep. 2013, doi: 10.1088/0031-9155/58/17/N241.

[60] K. Wake, I. Laakso, A. Hirata, J. Chakarothai, T. Onishi, S. Watanabe, V. De Santis, M. Feliziani, and M. Taki, "Derivation of coupling factors for different wireless power transfer systems: Inter- and intralaboratory comparison," *IEEE Trans. Electromagn. Compat.*, vol. 59, no. 2, pp. 677–685, Apr. 2017, doi: 10.1109/TEMC.2016.2636328.

[61] I. Laakso, A. Hirata, and O. Fujiwara, "Computational dosimetry for wireless charging of an electrical vehicle," in *Proc. Int. Symp. Electromagn. Compat.*, May 2014, pp. 202–205.

[62] Y. Tang, H. Ma, D. J. Thrimawithana, and U. K. Madawala, "Copper foil windings for WPT systems," in *Proc. IEEE PELS Workshop Emerg. Technologies: Wireless Power Transf. (WoW)*, May 2017, pp. 162–167, doi: 10.1109/WOW.2017.7959387.

[63] V. O. Adewuyi, "Overview and advancements in electric vehicle WPT systems architecture," in *Power Electronics, Radio Frequency and Microwave Engineering*. London, U.K.: IntechOpen, 2022, doi: 10.5772/intechopen.106254.

[64] X. Wang, J. Pang, Q. Tan, H. Dong, N. Zhao, and T. Xue, "Design of double-layer parallel printed spiral coil for wireless power transfer applied to rotating equipment," *Sens. Actuators A, Phys.*, vol. 331, Nov. 2021, Art. no. 112761, doi: 10.1016/j.sna.2021.112761.

[65] A. B. Diallo, M. Bensetti, C. Vollaire, L. Pichon, and A. Breard, "Scale reduction for modeling and prototyping of inductive power transfer system for EV applications," *IEEE Trans. Magn.*, vol. 59, no. 5, pp. 1–4, May 2023, doi: 10.1109/TMAG.2023.3239564.

[66] J. Pico, T. Bechtold, and D. Hohlfeld, "Model order reduction using COMSOL multiphysics software—A compact model of a wireless power transfer system," in *Proc. COMSOL Conf.*, 2016, pp. 4–6.
[67] J. Lan and A. Hirata, "Effect of loudspeakers on the in situ electric field in a driver body model exposed to an electric vehicle wireless power transfer system," *Energies*, vol. 13, no. 14, p. 3635, Jul. 2020, doi: 10.3390/en13143635.
[68] Y. Lim, H. Tang, S. Lim, and J. Park, "An adaptive impedance-matching network based on a novel capacitor matrix for wireless power transfer," *IEEE Trans. Power Electron.*, vol. 29, no. 8, pp. 4403–4413, Aug. 2014, doi: 10.1109/TPEL.2013.2292596.
[69] A. Kurs, A. Karalis, R. Moffatt, J. D. Joannopoulos, P. Fisher, and M. Soljačić, "Wireless power transfer via strongly coupled magnetic resonances," *Science*, vol. 317, no. 5834, pp. 83–86, Jul. 2007, doi: 10.1126/science.1143254.
[70] T. Campi, S. Cruciani, F. Maradei, and M. Feliziani, "Innovative wireless charging system for implantable capsule robots," *IEEE Trans. Electromagn. Compat.*, vol. 63, no. 5, pp. 1726–1734, Oct. 2021, doi: 10.1109/TEMC.2021.3078846.
[71] T. Campi, S. Cruciani, F. Maradei, and M. Feliziani, "Near-field reduction in a wireless power transfer system using LCC compensation," *IEEE Trans. Electromagn. Compat.*, vol. 59, no. 2, pp. 686–694, Apr. 2017, doi: 10.1109/TEMC.2016.2641383.
[72] M. Feliziani, T. Campi, S. Cruciani, F. Maradei, U. Grasselli, M. Macellari, and L. Schirone, "Robust LCC compensation in wireless power transfer with variable coupling factor due to coil misalignment," in *Proc. IEEE 15th Int. Conf. Environ. Electr. Eng. (EEEIC)*, Jun. 2015, pp. 1181–1186, doi: 10.1109/EEEIC.2015.7165335.
[73] P. Vishnuram, S. Panchanathan, N. Rajamanickam, V. Krishnasamy, M. Bajaj, M. Piecha, V. Blazek, and L. Prokop, "Review of wireless charging system: Magnetic materials, coil configurations, challenges, and future perspectives," *Energies*, vol. 16, no. 10, p. 4020, May 2023, doi: 10.3390/en16104020.
[74] *WE-FSFS Flexible Sintered Ferrite Sheet*. Accessed: Feb. 23, 2016. [Online]. Available: https://www.we-online.de/katalog/datasheet/354003.pdf
[75] T. Nagaoka, S. Watanabe, K. Sakurai, E. Kunieda, S. Watanabe, M. Taki, and Y. Yamanaka, "Development of realistic high-resolution whole-body voxel models of Japanese adult males and females of average height and weight, and application of models to radio-frequency electromagnetic-field dosimetry," *Phys. Med. Biol.*, vol. 49, no. 1, pp. 1–15, Jan. 2004, doi: 10.1088/0031-9155/49/1/001.
[76] S. Gabriel, R. W. Lau, and C. Gabriel, "The dielectric properties of biological tissues: III. Parametric models for the dielectric spectrum of tissues," *Phys. Med. Biol.*, vol. 41, no. 11, pp. 2271–2293, Nov. 1996, doi: 10.1088/0031-9155/41/11/003.
[77] I. Laakso, S. Tsuchida, A. Hirata, and Y. Kamimura, "Evaluation of SAR in a human body model due to wireless power transmission in the 10 MHz band," *Phys. Med. Biol.*, vol. 57, no. 15, pp. 4991–5002, Aug. 2012, doi: 10.1088/0031-9155/57/15/4991.
[78] I. Laakso and A. Hirata, "Fast multigrid-based computation of the induced electric field for transcranial magnetic stimulation," *Phys. Med. Biol.*, vol. 57, no. 23, pp. 7753–7765, Dec. 2012, doi: 10.1088/0031-9155/57/23/7753.
[79] A. Hirata, K. Yamazaki, S. Hamada, Y. Kamimura, H. Tarao, K. Wake, Y. Suzuki, N. Hayashi, and O. Fujiwara, "Intercomparison of induced fields in Japanese male model for ELF magnetic field exposures: Effect of different computational methods and codes," *Radiat. Protection Dosimetry*, vol. 138, no. 3, pp. 237–244, Mar. 2010, doi: 10.1093/rpd/ncp251.
[80] *Determining Procedures for the Measurement of Field Levels Generated by Electronic and Electrical Equipment in the Automotive Environment With Respect to Human Exposure*, document IEC 62764-1, 2022.
[81] I. Awai, Y. Zhang, T. Komori, and T. Ishizaki, "Coupling coefficient of spiral resonators used for wireless power transfer," in *Proc. Asia–Pacific Microw. Conf.*, Dec. 2010, pp. 1328–1331.
[82] J. Lan, Y. Diao, X. Duan, and A. Hirata, "Planar omnidirectional wireless power transfer system based on novel metasurface," *IEEE Trans. Electromagn. Compat.*, vol. 64, no. 2, pp. 551–558, Apr. 2022, doi: 10.1109/TEMC.2021.3123047.
[83] L. Tan, K. E. I. Elnail, M. Ju, and X. Huang, "Comparative analysis and design of the shielding techniques in WPT systems for charging EVs," *Energies*, vol. 12, no. 11, p. 2115, Jun. 2019, doi: 10.3390/en12112115.
[84] T. Hikage, Y. Kawamura, T. Nojima, and E. Cabot, "Numerical assessment methodology for active implantable medical device EMI due to magnetic resonance wireless power transmission antenna," in *Proc. Int. Symp. Electromagn. Compat. EMC Eur.*, Sep. 2012, pp. 1–6, doi: 10.1109/EMCEUROPE.2012.6396797.
[85] T. Campi, S. Cruciani, F. Maradei, and M. Feliziani, "Wireless charging of electric vehicles: Planar secondary coil position vs. Magnetic field," in *Proc. Int. Symp. Electromagn. Compat. EMC Eur.*, Sep. 2019, pp. 1116–1121, doi: 10.1109/EMCEurope.2019.8871775.

XIANYI DUAN (Student Member, IEEE) was born in Leshan, China, in 1992. She received the M.S. degree from Yamaguchi University, Yamaguchi, Japan, in 2020. She is currently pursuing the Ph.D. degree with the Department of Electrical and Mechanical Engineering, Nagoya Institute of Technology, Nagoya, Japan. Her research interests include electromagnetic safety, wireless power transfer, and related computational techniques.

JUNQING LAN (Member, IEEE) was born in Datong, China, in 1983. He received the Ph.D. degree in radio physics from Sichuan University, Chengdu, China, in 2013.

Since 2014, he has been an Assistant Professor with the Chengdu University of Information Technology, Chengdu. In 2019, he joined the Department of Electrical and Mechanical Engineering, Nagoya Institute of Technology, where he was an Assistant Professor. Currently, he is an Associate Professor with the Chengdu University of Information Technology. His current research interests include electromagnetic dosimetry modeling, wireless power transmission, and biological electromagnetic effects.

Dr. Lan is a member of IEEE ICES Standards Coordinating Committee.

SACHIKO KODERA (Member, IEEE) received the B.E. and M.E. degrees in electrical and computer engineering and the Ph.D. degree in computer science from the Nagoya Institute of Technology, Nagoya, Japan, in 2002, 2006, and 2019, respectively.

In 2016, she joined the Department of Electrical and Mechanical Engineering, Nagoya Institute of Technology, where she is currently an Associate Professor. Her current research interests include electromagnetic and thermal dosimetry modeling in humans for radio frequency and ambient heat exposures.

Dr. Kodera is a member of the Subcommittee 6 in Technical Committee 95 of IEEE International Committee on Electromagnetic Safety and the Scientific Expert Group of International Commission on Non-Ionizing Radiation Protection. She received the Prizes for Science and Technology (Public Understanding Promotion Category, in 2020) from the Commendation for Science and Technology, Minister of Education, Culture, Sports, Science, and Technology, Japan; and the Japan Open Innovation Prize (President of the Science Council of Japan Prize, in 2022) from the Cabinet Office.

JENS KIRCHNER (Senior Member, IEEE) received the Diploma degree in physics and the dual Ph.D. degrees in physics and philosophy from Friedrich-Alexander-Universität Erlangen-Nürnberg (FAU), Erlangen, Germany, in 2004, 2008, and 2016, respectively.

From 2008 to 2015, he was with Biotronik SE & Co. KG, in research and development of implantable cardiac sensors. Since 2015, he has been a Group Leader of medical electronics and multiphysical systems with the Institute for Electronics Engineering, FAU. His research interests include wearable sensor for chronic disease monitoring, bio-impedance measurement, inductive transcutaneous power transfer, and molecular communication.

Dr. Kirchner is a Senior Member of the IEEE with membership in the Communications Society, the Magnetics Society, and the Engineering in Medicine and Biology Society. He is also a member of EuMA.

GEORG FISCHER (Senior Member, IEEE) was born in Lower Rhine, in 1965. He received the degree in electrical engineering from RWTH Aachen University, Aachen, Germany, in 1992, with a special focus on communications, microwave/RF, and electro-dynamics, and the Dipl.-Ing. (TH) degree in electrical engineering and the Dr.-Ing. degree (summa cum laude) from the University of Paderborn, Paderborn, Germany, in 1992 and 1997, respectively, for a thesis on a polarization agile adaptive antenna array system for satellite communication.

From 1993 to 1996, he was a Research Assistant with the University of Paderborn. In 1996, he joined Bell Labs, Research of Lucent Technologies, Germany, focusing on base-station RF technology. He was promoted to a Bell Labs Distinguished Member of Technical Staff (DMTS), in 2000, and a Bell Labs Consulting Member of Technical Staff (CMTS), in 2001. In 2007, he was nominated for Bell Labs Fellow. In 2008, he was appointed as a Full Professor of electronics engineering with Friedrich-Alexander-Universität Erlangen-Nürnberg (FAU), Erlangen, Germany. His scientific research focuses on analog-digital balance of electronic systems. In medical, he researches wireless power transfer and wireless communication with implants, such as heart assistive devices. In power electronics, he is researching switch mode microwave power amplifiers.

Prof. Fischer is a member of EuMA and VDE and named inventor on more than 50 patents.

AKIMASA HIRATA (Fellow, IEEE) received the B.E., M.E., and Ph.D. degrees in communications engineering from Osaka University, Suita, Japan, in 1996, 1998, and 2000, respectively.

From 1999 to 2001, he was a Research Fellow with the Japan Society for the Promotion of Science, and a Visiting Research Scientist with the University of Victoria, Victoria, BC, Canada, in 2000. In 2001, he joined the Department of Communications Engineering, Osaka University, as an Assistant Professor. In 2004, he was an Associate Professor with the Department of Computer Science and Engineering, Nagoya Institute of Technology, where he is currently a Full Professor. His research interests include electromagnetic safety, risk management system for heat-related illness, methods in neuroscience, antennas, filters, and related computational techniques.

Prof. Hirata is a fellow of the Institute of Physics; and a member of IEICE, IEEE Japan, and Bioelectromagnetics Society. He received several awards, including the Young Scientists' Prize, in 2006; the Prizes for Science and Technology (Research Category, in 2011, and Public Understanding Promotion Category, in 2014 and 2020) by the Commendation for Science and Technology by the Minister of Education, Culture, Sports, Science, and Technology, Japan; and the IEEE EMC-S Technical Achievement Award in 2015; the Japan Academy Medal and JSPS Prize, in 2018; the Japan Open Innovation Prize (President of the Science Council of Japan Prize, in 2022) from the Cabinet Office; and the IEEE Richard R. Stoddart Award for Outstanding Performance, in 2023. He is also a member of the main commission, the Chair of project group of International Commission on Non-Ionizing Radiation Protection, a member of Administrative Committee, the Subcommittee (EMF Dosimetry Modeling) Chair of IEEE International Committee on Electromagnetic Safety, and an Expert of World Health Organization. From 2006 to 2012, he was an Associate Editor of IEEE TRANSACTION ON BIOMEDICAL ENGINEERING. He is an Editorial Board Member of *Physics in Medicine and Biology*.